

1 **Interference of Phosphate on the Adsorption of Arsenate and Arsenite Over**
2 **Confined Metastable 2-Line Ferrihyrite and Magnetite**

3 *Chennu Sudhakar,[†] Sritama Mukherjee,[†] Avula Anil Kumar,[†] Ganesan Paramasivam,[†] P.*

4 *Karthigai Meena,[†] Nonappa,[‡] and Thalappil Pradeep^{*†}*

5 [†] DST Unit of Nanoscience (DST UNS) and Thematic Unit of Excellence (TUE), Department of
6 Chemistry, Indian Institute of Technology Madras, Chennai 600036, India.

7 [‡] Faculty of Engineering and Natural Sciences, Tampere University, FI-33101, Tampere, Finland.

8
9 * Corresponding author

10 E-mail: pradeep@iitm.ac.in

24 **ABSTRACT**

25 Contamination of groundwater by arsenic (As(III/V)) is a serious global issue and
26 phosphate (P(V)) is known to be the biggest interference in adsorption-based remediation methods.
27 The present study is focused on understanding the interaction between phosphate and iron
28 oxides/oxy-hydroxides, with two well-known classes of potential adsorbents in the important pH
29 range of 5-9, and the effect of such interactions on the uptake of arsenite and arsenate.
30 Spectroscopic studies such as XPS and FTIR were used to understand the binding of various
31 oxyanions of phosphorous and arsenic with the iron oxides/oxy-hydroxides, exploring the core
32 levels of P 2p and Fe 2p. Materials used for adsorption experiments were magnetite (MAG) and a
33 nanocomposite, confined metastable 2-line ferrihydrite (CM2LF)); CM2LF is used for arsenic
34 remediation in the affected states of India. Further, we studied the interference of P(V) on As(III/V)
35 adsorption. Kinetics of adsorption was quantified using ion chromatography (IC), where P(V)
36 alone followed a pseudo-second-order model. In the case of mixed solutions, namely, AP_{mix1} (P(V)
37 + As(III)) and AP_{mix2} (P(V) + As(V)), kinetics data suggested that P(V) or As(III/V) oxyanions are
38 partially following the pseudo-second-order model. Results also confirmed that CM2LF
39 performed better than magnetite (MAG) for As(III/V) uptake in presence of P(V). As(III) and
40 As(V) species are more competitive than P(V) at neutral pH. A model for the adsorption of P(V)
41 species in water on a ferrihydrite particles was developed using DFT. This accounted for phosphate
42 complexation at various pH values. The study is highly useful in developing an affordable solution
43 for sustainable arsenic remediation. Various aspects of sustainability were discussed.

44

45 **KEYWORDS:** arsenite, arsenate, phosphate, CM2LF, magnetite, adsorption kinetics.

46

47

48

49

50

51

52 INTRODUCTION

53 Phosphorus (P) is the 11th most common element and is essential for all known life forms on
54 earth.¹⁻² It exists in different inorganic and organic forms having various oxidation states (+V, +III,
55 +I, 0, and -III). The dominant biological forms of P are $\text{H}_2\text{PO}_4^{1-}$, HPO_4^{2-} and PO_4^{3-} at biologically
56 relevant pH (7-9).³ There are similarities between P and arsenic (As). Arsenic is a metalloid that
57 sits just below P in the periodic table with larger atomic radii, with the same number of valence
58 electrons, and nearly identical electronegativity. Arsenic exists preferentially in +V, +III, and 0
59 oxidation states. The similarity between phosphorus and arsenic translates to various species they
60 form, importantly phosphate (PO_4^{3-}) and arsenate (AsO_4^{3-}). The dissociation constants for P(V) in
61 H_3PO_4 are close to As(V) in H_3AsO_4 over a range of physiological conditions. Also, As(V) can
62 retain a negative charge even when it bonds to two other species, similar to P(V). Due to these
63 similarities, As(V) and P(V) are not easily distinguishable by most life forms³. As(V) is taken up
64 by cells via phosphate transporters and can substitute for P(V) in the early steps of many
65 phosphate-based metabolic pathways.³

66 Interaction of arsenic with metal oxides or metal oxy-hydroxides is mainly influenced by pH (H^+ /
67 OH^- ions) and competing ions (phosphates, silicate, iron, manganese, calcium, magnesium, nitrate,
68 chloride, and sulfate), generally present in groundwater.⁴ The mobility of these oxyanions (P(V),
69 As(III/V)) in the environment is influenced by redox potential, pH conditions, organic matter, and
70 other competing oxyanions.⁵ Phosphate can interact with iron oxide surfaces through Fe-O-P
71 bonds. These are relevant processes in bacterial adhesion as in the case of organisms such as
72 *Bacillus subtilis* and *Pseudomonas aeruginosa*.⁶ Phosphate and arsenate are considered to have
73 similar adsorption characteristics because they have very similar protonation tendency in aqueous
74 medium.⁷⁻¹⁰ Due to their structural similarities, PO_4^{3-} competes with AsO_4^{3-} during sorption and
75 coprecipitation on iron oxy-hydroxides.¹¹⁻¹⁴ The presence and mobility of contaminants (in the
76 context of arsenic and other heavy metal ions) in groundwater systems are strongly dependent on
77 the interaction with iron and aluminum-based materials present in soils and waterways.¹⁵ Studies
78 on the desorption of arsenic compounds were reported in the presence of PO_4^{3-} and Cl^- and other
79 constituents.¹⁶

80 While numerous PO_4^{3-} adsorption studies have been performed in view of its importance to soil¹⁷,
81 in water it is treated as a pollutant depending on its concentration levels.¹⁸ For its removal, the

82 adsorbents used are mainly iron oxides (hematite¹⁹ and magnetite²⁰⁻²¹) and iron oxy-hydroxides
83 (ferrihydrite²², goethite²³, and maghaemite²⁴). Adsorption of phosphate onto iron oxides/oxy-
84 hydroxides (commonly present in soils) plays a significant role in soil fertility as it influences the
85 surface charge responsible for attachment of organic matter to the soils.²³ The effect of pH on
86 various complexation mechanisms, such as inner-sphere and outer-sphere adsorption on the
87 hematite surface, were reported.²⁵ The molecular-scale structure of surface complexes depends on
88 the mineral surfaces and there is a brief discussion on models of surface complexation in Wang et
89 al. 2013.²⁶ Sodium phosphate interaction with iron oxide (Fe₂O₃) was understood by using density
90 functional theory (DFT) calculations.²⁷ Adsorption of phosphate on ferrihydrite¹⁵/magnetite²⁸ has
91 been studied using X-ray photoelectron spectroscopy (XPS). Earlier, attenuated total reflectance-
92 Fourier transform infrared spectroscopy (ATR-FTIR) was also used to study the influence of
93 phosphate on the adsorption of As(V) on goethite and ferrihydrite.²⁹ Binary oxy-hydroxide such
94 as Fe and Mn-based mixed oxy-hydroxide was used to study the competitive adsorption of arsenate
95 and phosphate.³⁰ This suggest that the adsorption of arsenate (6-80 μM) on binary oxy-hydroxide
96 decreased approximately 7-20% in presence of P(V) (120-300 μM). Even after considerable
97 research, phosphate interference during arsenic adsorption is not well understood and needs a more
98 comprehensive effort.

99 Present work focuses on the elucidation of phosphate adsorption and its interference in arsenic
100 uptake on MAG and CM2LF substrates in qualitative and quantitative manner. Experiments were
101 conducted with different ionic forms of P and As. CM2LF is a nanoscale material that has been
102 developed in our lab and is being used to supply arsenic-free water to over 1.2 million people every
103 day. All adsorption experiments were conducted in the environmentally relevant pH range of 5-9.
104 While XPS and IR spectroscopy were performed to have a detailed understanding of the surface
105 complexation phenomena during adsorption, all uptake experiments were quantified using ion
106 chromatography (IC) and inductively coupled plasma-mass spectrometry (ICP-MS). Finally, DFT
107 calculations were performed on various phosphate complexes at model surfaces, such as bidentate
108 binuclear (²C) [$>(\text{FeO})_2(\text{OH})\text{PO}$ or $>(\text{FeO})_2(\text{OH})_2\text{P}$], bidentate mononuclear (²E) [$>\text{FeO}_2(\text{OH})\text{PO}$
109 or $>\text{FeO}_2(\text{OH})_2\text{P}$], monodentate mononuclear (¹V) [$>\text{FeO}-\text{PO}_2(\text{OH})$ or $>\text{FeO}-\text{PO}(\text{OH})_2$], and
110 physically adsorbed species (T) [$>\text{FeOH}\dots\text{O}-\text{PO}_2(\text{OH})$ or $>\text{FeO}\dots\text{HO}-\text{PO}_2(\text{OH})$] to support the
111 XPS results. ²C, ²E, and ¹V are referred to as inner-sphere complexes and T is referred to as an

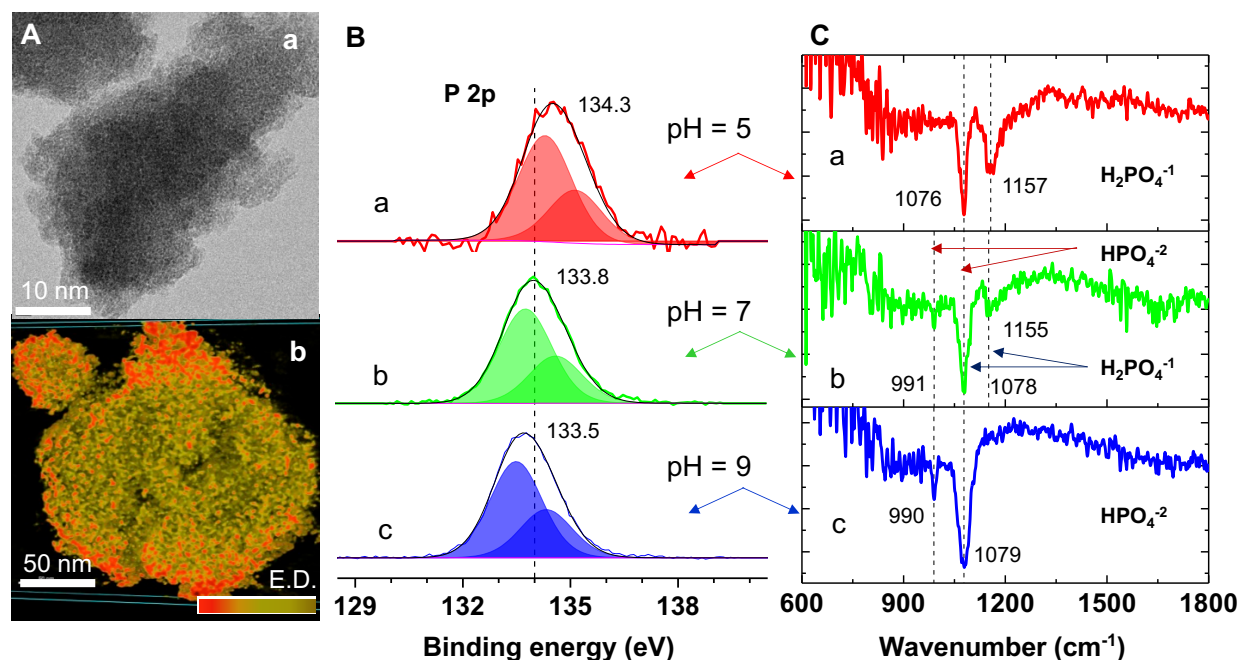
112 outer-sphere complex. Also, a brief discussion is given on the sustainability aspects of both the
113 materials.

114

115 **EXPERIMENTAL SECTION**

116

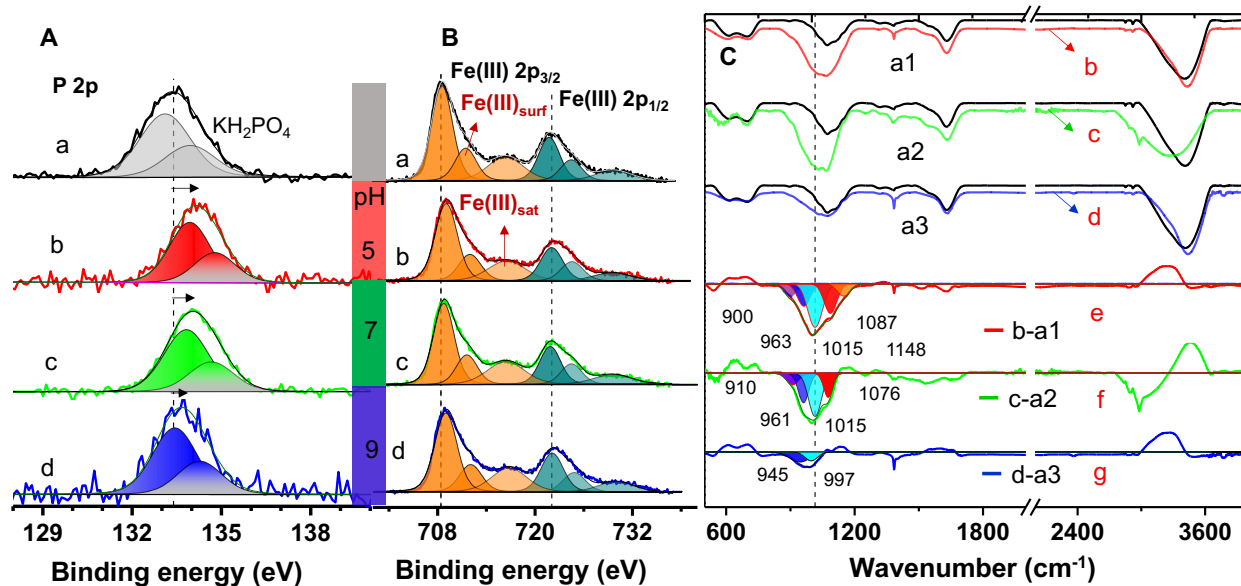
117 Stock solutions of 100 mM P(V), As(III), and As(V) were prepared using KH_2PO_4 , NaAsO_2 , and
118 $\text{Na}_2\text{HAsO}_4 \cdot 7\text{H}_2\text{O}$ salts, respectively. P(III) was not examined as it is not a dominant form in the
119 environment. A combination of P(V) and As(III) is referred to as AP_{mix1} and mixture of P(V) and
120 As(V) is referred to as AP_{mix2} . A 100 mM AP_{mix1} stock solution was prepared by mixing equimolar
121 amounts of NaAsO_2 and KH_2PO_4 . The mixture, AP_{mix2} was made with equimolar quantities of
122 $\text{Na}_2\text{HAsO}_4 \cdot 7\text{H}_2\text{O}$ and KH_2PO_4 . The pH of the stock solutions was adjusted to 7 by adding dil. HCl
123 or dil. NaOH, whenever necessary. Further, 150 mg of CM2LF was added to 100 mL of 40 mM
124 solutions of P(V), AP_{mix1} , and AP_{mix2} , each in 250 mL polypropylene conical flasks. The same
125 process was followed for the MAG material. The flask was held on an orbital shaker for 24 h until
126 an adsorption equilibrium was reached. The solution was centrifuged, and the residue (adsorbent)
127 was washed several times with deionized water to remove unreacted species (P or As) from the
128 surface of the material. Thereafter, about 2-3 mg of the cleaned residue was suspended in 300 μL
129 distilled water for sample preparation for XPS, and similar sample preparation was done for IR.
130 The suspension was dropcast on 1 cm x 1 cm ITO-plate (non-conducting surface) which was kept
131 in a vacuum desiccator for 48 h for complete drying and to prevent contamination. For clear
132 understanding of the kinetics of phosphate uptake and its interference on arsenic adsorption
133 kinetics, IC and ICP-MS measurements were performed. For this, 100–150 mg of CM2LF was
134 added to 5–20 ppm of 100 mL of P(V), AP_{mix1} , and AP_{mix2} solutions each in a 250 mL
135 polypropylene conical flask. The same process was followed for MAG. The solution was held on
136 an orbital shaker, and 1 mL of the solution was collected at various time intervals at 3, 5, 10, 15,
137 20, 40, 60, and 90 min, respectively. The solutions were subjected to centrifugation immediately
138 after collecting them. The material if any, separated as residue, was discarded and the supernatant
139 was filtered using a 0.2 μm membrane filter and the filtrate was diluted to 5 ml using millipore
140 water of 18 M Ω resistance. Details about materials, instrumentation and computational aspects are
141 provided in Supporting Information.



143
 144 **Figure 1.** (A) a) TEM image and b) 3D reconstructed tomographic image of 2-line ferrihydrite
 145 composite (CM2LF), E.D. means electron density. (B) XPS P 2p spectra of aqueous phosphate
 146 solutions at various pH: a) 5, b) 7, and c) 9 after drying. The XPS samples were prepared by drop
 147 casting the phosphate solutions onto an ITO-plate and dried at room temperature for two days. (C)
 148 ATR-FTIR spectra of 100 mM phosphate at various pH: a) 5, b) 7, and c) 9 in the region of interest.
 149 All IR spectra shown here were subtracted from that of water.

150
 151 Figure 1Aa shows a TEM image of CM2LF. The image suggests that the material is composed of
 152 amorphous particles, in agreement with the literature.³¹ To further investigate the morphology of
 153 the CM2LF aggregates, transmission electron tomographic reconstruction was performed for
 154 CM2LF and its composites with As(III) and As(V). Accordingly, a series of 2D projections were
 155 collected between $\pm 69^\circ$ with 3° increment (see Supporting Information 2 for details). 3D
 156 reconstruction of CM2LF suggests that the material has a porous structure with random
 157 aggregation but with no well-defined packing patterns (Figure 1Ab; Figures S1Ai and S1Aii). Such
 158 random aggregation and porous structure are beneficial for the uptake of various species like
 159 As(III/V) and P(V). Further, the tomographic reconstruction of As(III/V) bound CM2LF

160 nanoparticles show no change in the morphological features (Figures S1Bi and S1Bii for As(III)
161 adsorbed CM2LF, and Figures S1Ci and SCii for As(V) adsorbed CM2LF). This suggests that the
162 structures are intact even after As(III/V) binding. XPS and FTIR spectra of phosphate species were
163 measured at pH 5, 7, and 9 to understand the degree of protonation and phosphate speciation at
164 room temperature. P 2p energy levels of phosphate species are shifted to lower binding energies
165 ($134.3 > 133.8 > 133.5$ eV) with increase in pH (Figure 1B). Note that the XPS spectra were
166 measured in the dry state of materials. The materials, magnetite^{28, 32-33} and 2-line ferrihydrite^{12, 34}
167 nanoparticles embedded into organic matter (chitosan and cellulose) are stable in the pH range of
168 5-9. Previous spectroscopic (XPS and Mossbauer) studies suggest that phosphate adsorbed wet
169 magnetite nanoparticles remain as magnetite after drying.^{28, 32-33} Kumar et al. studied arsenic
170 adsorbed CM2LF (in dry state) using X-ray powder diffraction and electron energy-loss
171 spectroscopy.³¹ These studies demonstrated that there is no phase change in 2-line ferrihydrite.
172 These materials get converted from one phase to another, taking months or years under natural
173 circumstances. However, the current study doesn't target studying the dehydration³⁵, surface
174 reactivity³⁶, and aggregation³⁶⁻³⁷ of the bare 2-line ferrihydrite nanoparticles. We dried the wet
175 (after adsorption) samples at room temperature (24-30°C) for measurements. These experimental
176 conditions cannot affect the chemical state of the elements (P, Fe and As). Magnetite and CM2LF
177 materials are stable even above 80°C. Considering the previous reports, XPS data are valuable for
178 identifying chemical states and for quantifying the elements, although the samples were dried prior
179 to measurements. XPS data of each peak before and after the interaction of P(V)/AP_{mix1}/AP_{mix2}
180 with CM2LF and MAG used in this work are shown in Supporting Information, Table S1.
181 Deprotonation of hydroxyl groups attached to P causes an increase in the electron density on O
182 atoms (P-OH to P-O⁻), which results in an increase in the electron density on P atom. This change
183 leads to a fall in the BE of P 2p. These results are supported by theoretical calculations (Table S2).
184 P(V) in solution at pH 5 has two vibrational features at 1076 and 1157 cm⁻¹ (Figure 1Ca). These
185 correspond to the symmetric stretching frequencies of -P-OH and -P=O of H₂PO₄¹⁻, with C_{2v}
186 structure.^{22, 38} At pH 9, it shows two features at 990 and 1079 cm⁻¹ (Figure 1Cc) corresponding to
187 the bending of -PO₂ and symmetric stretching of -P-OH groups of HPO₄²⁻, with C_{3v} structure.^{22, 38}
188 However, at pH 7, P(V) shows three characteristic peaks at 1155, 1078, and 991 cm⁻¹ (Figure 1Cb)
189 due to H₂PO₄¹⁻ and HPO₄²⁻.

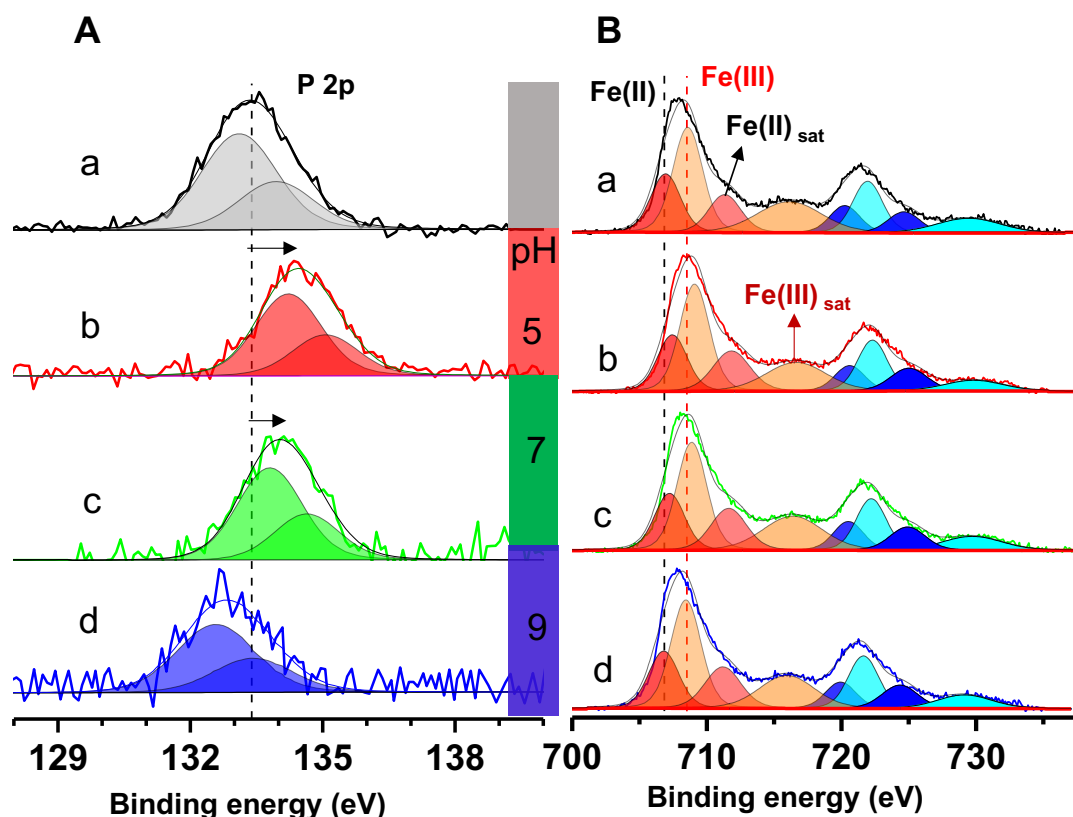


190
 191 **Figure 2.** XPS spectra of (A) P 2p region of a) KH_2PO_4 solid, adsorbed phosphate on CM2LF at
 192 various pH: b) 5, c) 7, and d) 9. (B) The Fe 2p region showing $2p_{3/2}$ and $2p_{1/2}$ features of a) CM2LF
 193 before adsorption, (b–d) Fe 2p after phosphate adsorption at various pH: 5, 7, and 9. (C) FTIR
 194 spectra of CM2LF before adsorption, it was treated with distilled water, adjusted to various pH:
 195 a1) 5, a2) 7, and a3) 9. FTIR spectra of CM2LF measured after phosphate adsorption at pH b) 5,
 196 c) 7, and d) 9, respectively. The difference between the FTIR features before and after phosphate
 197 adsorption at various pH: 5, 7, and 9 were represented by curves e), f), and g), respectively. Various
 198 component features observed in the difference spectra are also shown.

199 **Adsorption on CM2LF:**

200 The XPS analysis of phosphate standard in the solid form (KH_2PO_4) is shown in Figure 2Aa. The
 201 P 2p peak for it appears at 133.4 eV. The P 2p peak was deconvoluted into $2p_{3/2}$ and $2p_{1/2}$. The P
 202 2p was shifted from 133.4 (KH_2PO_4) to 134.2, 134.1, and 133.9 eV upon its adsorption on CM2LF
 203 at pH 5, 7, and 9, respectively. Throughout this paper, blueshift indicates that the selected peak
 204 shifted to higher binding energy from a reference peak, and redshift indicates the opposite. Large
 205 blueshift was observed at pH 5 (0.8 eV) and 7 (0.7 eV) (Figures 2Ab and 2Ac). This suggests that
 206 P(V) forms more stable inner-sphere complexes (^2C) at pH 5 and 7. On the other hand, a small
 207 blueshift was observed for pH 9 (Figure 2Ad), indicating that there are some amount of outer-
 208 sphere complexes (T) along with inner-sphere complexes. In contrast, may be P(V) forms more
 209 number of less stable inner-sphere complexes (^2E and ^1V). However, there is more chance of

210 forming outer-sphere complexes at pH 9 due to the increase of Fe–O⁻ groups. A minor change
211 observed in the position of P 2p peak while comparing with pH 5 and 7 arise due to the variation
212 in the extent of protonation of surface complexes. Figure 2Ba shows Fe 2p fitted with three pairs
213 of peaks of CM2LF³⁹. The lowest binding energy corresponds to –Fe–O–Fe– groups, the next
214 refers to the surface >Fe–OH groups (Fe(III)surf) followed by a satellite peak (Fe(III)sat). A
215 significant blueshift was observed in Fe 2p due to adsorption of P(V) at various pH, as shown in
216 Supporting Information, Table S1. The shifted peaks did not match with Fe 2p of Fe(II) and Fe(IV)
217 ions. Thus the Fe 2p data suggest that there was no reduction or oxidation of iron (Fe(III)) upon
218 P(V) uptake (Figure 2B). The observed blueshift in Fe 2p is due to the formation of inner-sphere
219 complexes (–Fe–O–P–), which are to be discussed in Figure 7. FTIR spectroscopic studies were
220 used to identify the inner-sphere complexes of P(V) with CM2LF. At first, we studied pH influence
221 on CM2LF in the range of 4-9 using FTIR. The results suggest that CM2LF functional groups are
222 not affected by varying pH (Supporting Information, Figure S2). The IR spectrum at pH 5 (Figure
223 2Ce) was fitted with five peaks: 900, 963, 1015, 1087, and 1148 cm⁻¹. The 1015 cm⁻¹ was assigned
224 to –Fe–O–P–, 1148 cm⁻¹ to P=O stretching, 1087 cm⁻¹ to PO₂ group, while 900 and 963 cm⁻¹
225 corresponded to P-OH symmetric bending vibrations. These features refer to bidentate binuclear
226 (²C) species [²(FeO)₂(OH)PO or ²(FeO)₂(OH)₂P].^{22, 38, 40} These features also correspond to C₁
227 symmetry complexes. In previous reports, at pH 4.5, the formation of less stable inner-sphere
228 complexes (²E and ¹V) were observed⁴¹ when P(V) loadings were increased from 1.25 to 10
229 μmol/m² (μmol/m² ≈ ppb), i.e., higher P(V) loading increases the chance of formation of less stable
230 complexes (²E and ¹V). Here P(V) loadings used were higher than 10 μmol/m². Thus there may be
231 some amount of ²E and ¹V complexes. The spectrum observed at pH 7 (Figure 2Cf) shows four
232 features at 910, 961, 1015, and 1076 cm⁻¹ that refer to bidentate binuclear species
233 [²(FeO)₂(OH)PO].^{22, 34} The pH 9 spectrum (Figure 2Cg) shows only two features at 945 and 997
234 cm⁻¹. These features are similar to 961 and 1015 cm⁻¹ features (at pH 5) with shift (16 cm⁻¹) that
235 may correspond to deprotonated bidentate binuclear species [²(FeO)₂PO₂]. However, from these
236 data, it is difficult to understand exact surface complexes. XPS data confirm that the CM2LF
237 surface is covered with more outer-sphere complexes than inner-sphere complexes at pH 9 (Figure
238 2Ad).



239

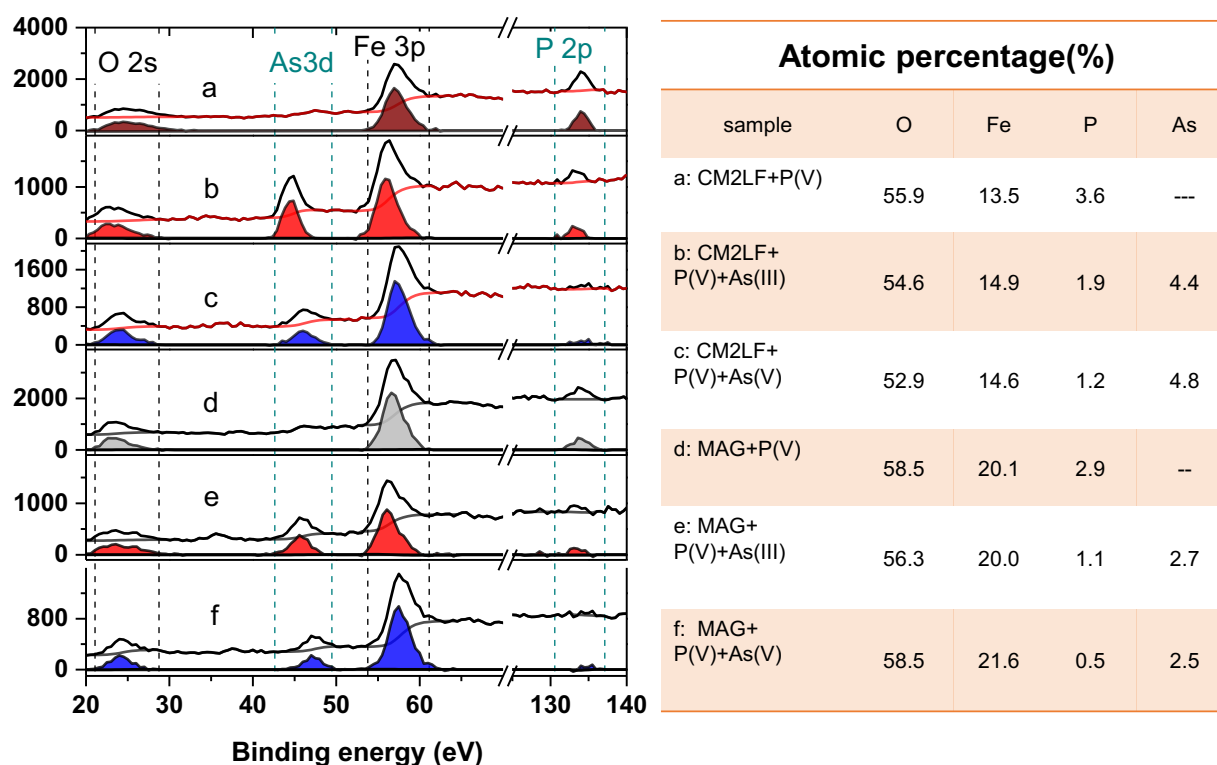
240

241 **Figure 3.** XPS spectra of (A) P 2p region of a) KH_2PO_4 solid, adsorbed phosphate on MAG at
 242 various pH: b) 5, c) 7 and d) 9. (B) Fe 2p region showing $2p_{3/2}$ and $2p_{1/2}$ features of a) MAG before
 243 adsorption, (b–d) after adsorption at pH 5, 7, and 9, respectively.

244 **Adsorption on MAG:**

245 In the case of MAG, the Fe $2p_{3/2}$ was deconvoluted into four peaks which correspond to Fe(II),
 246 Fe(III), and two separate shake-up peaks for Fe(II) (Fe(II)sat) and Fe(III) (Fe(III)sat).^{39, 42}
 247 Similarly, deconvolution was done for Fe $2p_{1/2}$. The Fe $2p_{3/2}$ (for Fe(II) and Fe(III)) feature of
 248 MAG appears at 707.9 eV before phosphate adsorption (Figure 3Ba), and after adsorption, it is
 249 blueshifted by 0.6 and 0.4 eV at pH 5 and 7, respectively and no shift was observed in the case of
 250 pH 9 (Figures 3Bd). The shifts are shown in Supporting Information, Table S1. Upon P(V)
 251 interaction with MAG at various pH, considerable change was observed in P 2p. The P 2p was
 252 shifted from 133.4 (KH_2PO_4) to 134.5, 134.0, and 132.8 eV at pH 5, 7, and 9, respectively when
 253 P(V) interacted with MAG (Figure 3A). The P 2p is more blueshifted at pH 5 and less at pH 7

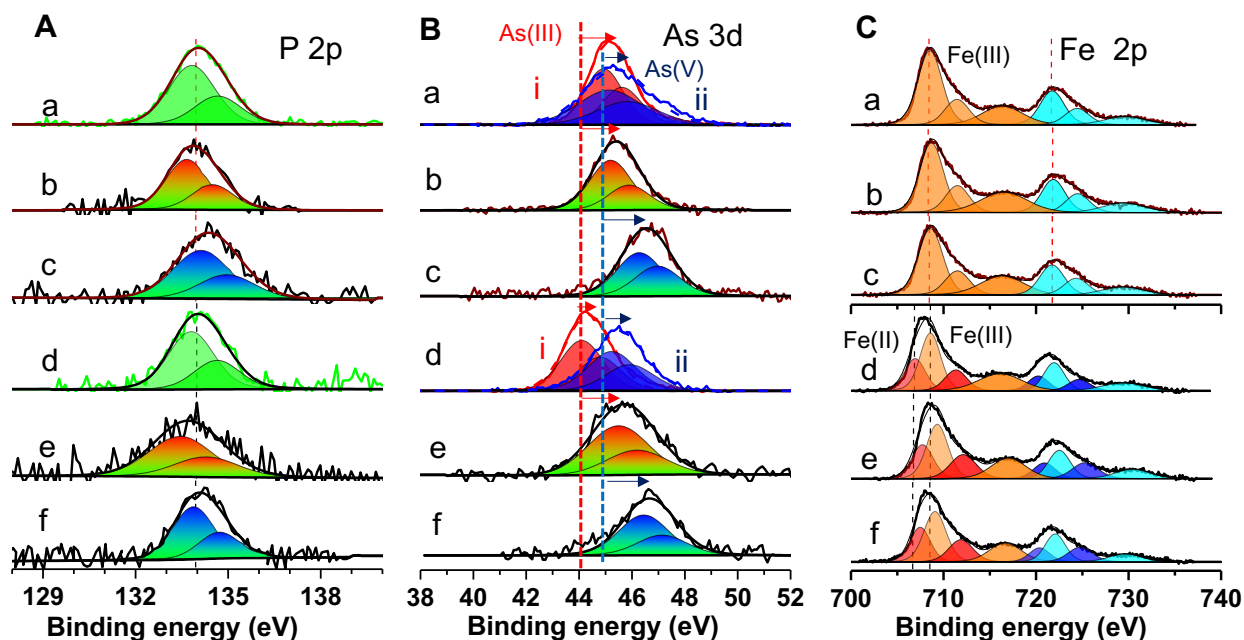
254 (Figures 3Ab and 3Ac). These results are similar to that of CM2LF which suggest that phosphate
 255 forms monoprotonated bidentate binuclear (²C) species at pH 5 and 7.²⁸ According to the literature,
 256 the P 2p binding energy for adsorbed phosphate on magnetite is 133.6 eV when the P(V) uptake
 257 is in the range of 2-5 mg/g.²⁸ Previous FTIR and Mossbauer spectroscopic studies reflected that
 258 phosphate is attached to Fe(III) at the octahedral sites as monoprotonated bidentate binuclear
 259 complexes.²⁸ At pH 9, P 2p of the adsorbed phosphate shows a shift towards lower binding energy
 260 as compared to the KH₂PO₄ (Figures 3Ad and 3Aa). No shift was observed in Fe 2p_{3/2} peak upon
 261 P(V) uptake as discussed before. The results at pH 9 suggest that most of the species are adsorbed
 262 through hydrogen bonding (outer-sphere complexes or physically bonded species). The physically
 263 bonded (T) species are having lower P 2p binding energy compared to inner-sphere complexes.
 264 The binding energy of P 2p of various phosphate complexes (²C, ²E, ¹V and T) were calculated
 265 from theoretical studies (see Figure 7).
 266



267
 268 **Figure 4.** XPS spectra of CM2LF treated with a) P(V), b) AP_{mix1} and c) AP_{mix2} and MAG treated
 269 with d) P(V), e) AP_{mix1}, and f) AP_{mix2}. The spectra shows the regions corresponding to O 2s (20-
 270 28 eV), As 3d (40-50 eV), Fe 3p (52-60 eV), and P 2p (130-136 eV). The atomic compositions of

271 O, As, Fe and P in the materials were calculated after adsorption from the corresponding XPS
 272 spectrum; the values are presented in the table on the right.

273 The atomic percentage (Figure 4) shows the interference of of P(V) in the adsorption of arsenic
 274 (As(III/V)) while each had a concentration of 20 mM. The P(V) uptake is higher for CM2LF
 275 (3.6%) than for magnetite (2.9%) (Figures 4a and 4d, respectively). In the case of mixtures (AP_{mix1}
 276 and AP_{mix2}), CM2LF (Figures 4b and 4c) shows better As(III/V) uptake capacity than magnetite
 277 (Figures 4e and 4f). This can be attributed to lower number of adsorption sites (Fe—OH₂⁺, Fe—
 278 OH) available in magnetite than CM2LF. The porous structure of CM2LF provides additional
 279 adsorption sites, as shown in Figure 1Ab. At pH 7, in the case of AP_{mix1}, the component As(III)
 280 and in the case of AP_{mix2}, the component As(V) were more adsorbed on CM2LF/MAG than P(V)
 281 (Figures 4b and 4e; Figures 4c and 4f). The complexation of phosphate in presence of As(III/V)
 282 was further evaluated by studying the energy levels of P 2p, As 3d, and Fe 2p (Figure 5).



283
 284 **Figure 5.** XPS spectra of (A) P 2p, (B) As 3d, and (C) Fe 2p. In (A) P 2p region, CM2LF treated
 285 with a) P(V), b) AP_{mix1}, and c) AP_{mix2}, and MAG treated with d) P(V), e) AP_{mix1}, and f) AP_{mix2},
 286 respectively are presented. In the As 3d region (B), the red and blue traces correspond to NaAsO₂
 287 and Na₂HAsO₄·7H₂O. Only As(III) adsorbed materials are ai) CM2LF and di) MAG, and on the
 288 other hand, As(V) adsorbed materials are aii) CM2LF and dii) MAG. Traces b and c, e and f are

289 after adsorption of ions while using mixed solutions (AP_{mix1} and AP_{mix2}) as indicated above. In (C)
290 Fe 2p region, a) CM2LF and d) MAG before adsorption, and remaining (b and c, e and f) are after
291 adsorption of ions while using mixed solutions, as above.

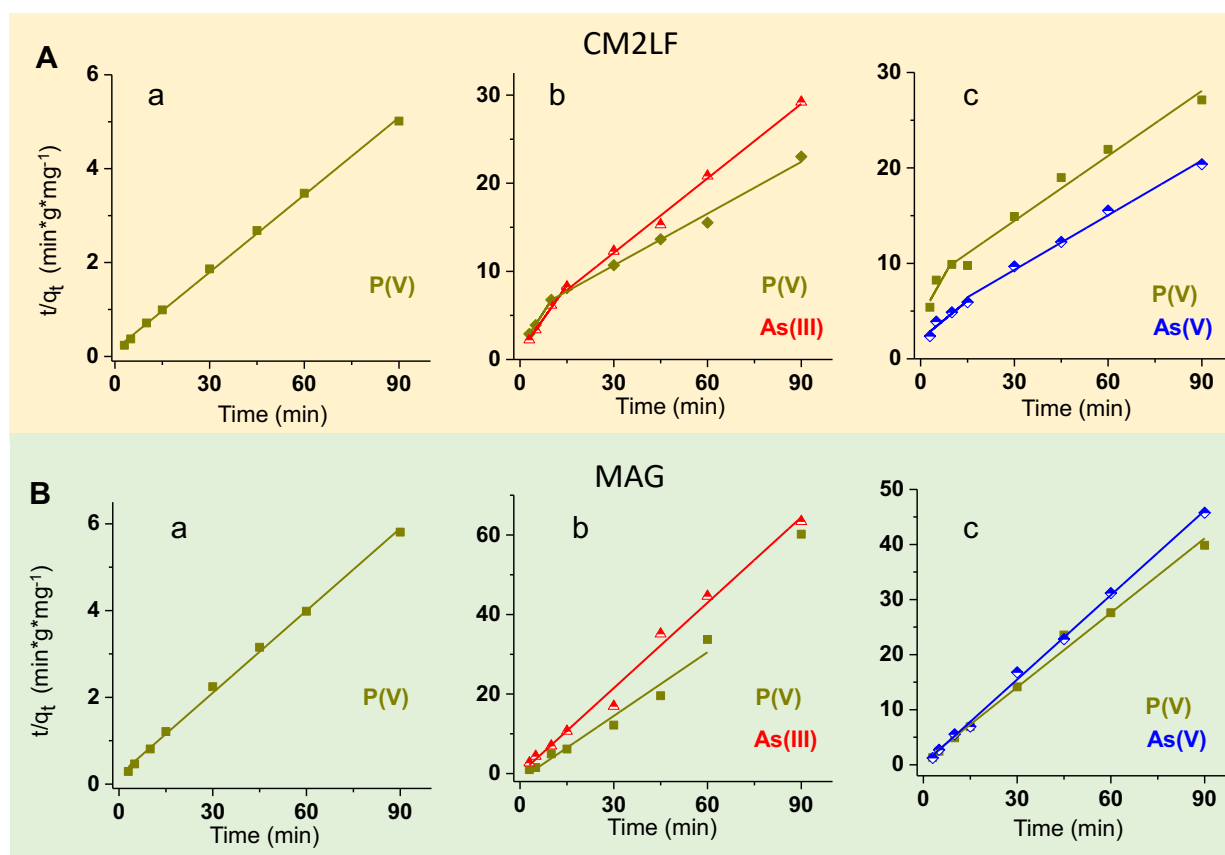
292 In the case of CM2LF, there is no considerable shift observed in the P 2p peak between P(V) and
293 AP_{mix1} ($P(V) = 134.0$, $AP_{mix1} = 134.1$ eV (Figures 5Aa and Ab)), and while looking at the
294 corresponding As 3d region for AP_{mix1} , which showed a peak at 45.4 eV (Figure 5Bb), this is
295 slightly blueshifted from As(III) treated sample (45.1 eV (Figure 5Bai)). This blueshift indicates
296 that the ratio of inner-sphere to outer-sphere complexes of As(III) is more in the case of AP_{mix1}
297 than As(III) alone. Corresponding IR spectrum (Supporting Information, Figure S3d) shows
298 features at 790, 830, 886, 970, 1010, and 1075 cm^{-1} , where the features at 790 cm^{-1} belongs to As-
299 OH stretching, 830 cm^{-1} due to Fe-O-As bonds, 1075 cm^{-1} due to PO_2 group, 970 cm^{-1} due to P-
300 OH, and 1010 cm^{-1} to -Fe-O-P. IR data suggest that P(V) and As(III/V) are chemisorbed when they
301 were co-adsorbed. Hence, XPS data suggest P(V) interference in As(III) complexation.

302 A slight red shift was observed in P 2p peak in the case of AP_{mix1} adsorption ($AP_{mix1} = 133.7$ eV,
303 Figure 5Ae) as compared to P(V) adsorption ($P(V) = 134.1$ eV, Figure 5Ad) on the MAG surface.
304 This shift refers to physically adsorbed species. Thus there are some amount of physically adsorbed
305 phosphate species on the surface of MAG along with chemically adsorbed species at pH 7. The
306 AP_{mix1} treated MAG shows As 3d peak at 45.7 eV, and it is more blueshifted as compared to
307 As(III) alone (44.3 eV) (Figures 5Be and 5Bdi). The observed shift is high (1.4 eV), which suggests
308 that there are greater fraction of chemically adsorbed species in the case of AP_{mix1} compared to
309 As(III) alone (in overall surface complexes). Thus, there is a positive effect on As(III)
310 complexation in presence of P(V), but vice versa is not true.

311 While comparing AP_{mix2} treated CM2LF and P(V) treated CM2LF, there is a noticeable shift (0.3
312 eV) observed in P 2p; the P 2p peaks are at 134.4 and 134.1 eV, respectively (Figures 5Ac and
313 5Aa). This may be due to the increased ratio of inner to outer-sphere complexes or a plausible
314 conversion of less stable inner-sphere complexes (1V) to more stable inner-sphere complexes (2C)
315 of P(V) in presence of As(V). For the As 3d region of AP_{mix2} (Figure 5 Bc) and As(V) (Figure
316 5Baii) treated CM2LF, the peaks are at 46.5 and 45.3 eV. The shift between them is 1.2 eV, which
317 suggests increased chemisorption of As(V) in presence of P(V) than As(V) alone. The
318 corresponding IR spectrum (Supporting Information, Figure S3e) shows two features at 820 and

319 871 cm^{-1} ; 820 cm^{-1} is assigned to Fe-As-O- bond stretching and 871 cm^{-1} is due to As=O; these
320 features correspond to stable inner-sphere complexes (^2C).

321 However, in the case of $\text{AP}_{\text{mix}2}$ treated MAG, no shift was observed in P 2p as compared to $\text{AP}_{\text{mix}2}$
322 treated MAG and P(V) treated MAG at pH 7 ($\text{AP}_{\text{mix}2} = 134.1$ eV, P(V) = 134.1 eV (Figures 5Af
323 and 5Ad)). As(V) shows a 3d peak at 46.6 eV (Figure 5Bf). The results are the same as in the case
324 of CM2LF. Hence, similar complexes (^2C or ^3C (tridentate trinuclear complex)) can be expected
325 here. These results suggest that the ratio of inner to outer sphere complexation of As(III/V)
326 increases in presence of P(V). On the other hand, these results may be obtained due to strong
327 hydrogen-bonding to surrounding ferric hydroxyl groups (-Fe-OH) or arsenic hydroxyl groups (-
328 As-OH). The consolidated results are presented in Table S3 in Supporting Information.



329
330 **Figure 6.** Pseudo-second-order kinetics plot for adsorption of a, b, and c indicating phosphate,
331 $\text{AP}_{\text{mix}1}$, and $\text{AP}_{\text{mix}2}$, respectively on (A) CM2LF and (B) MAG. The q_t of each data point was
332 evaluated using linear form of pseudo-second-order equation where unit of q_t is mg/g . In the case

333 of CM2LF treated with AP_{mix1} and AP_{mix2} adsorption kinetics data gave two slopes from 0 to 10
 334 min and 15 to 90 min indicating varying rates of adsorption.

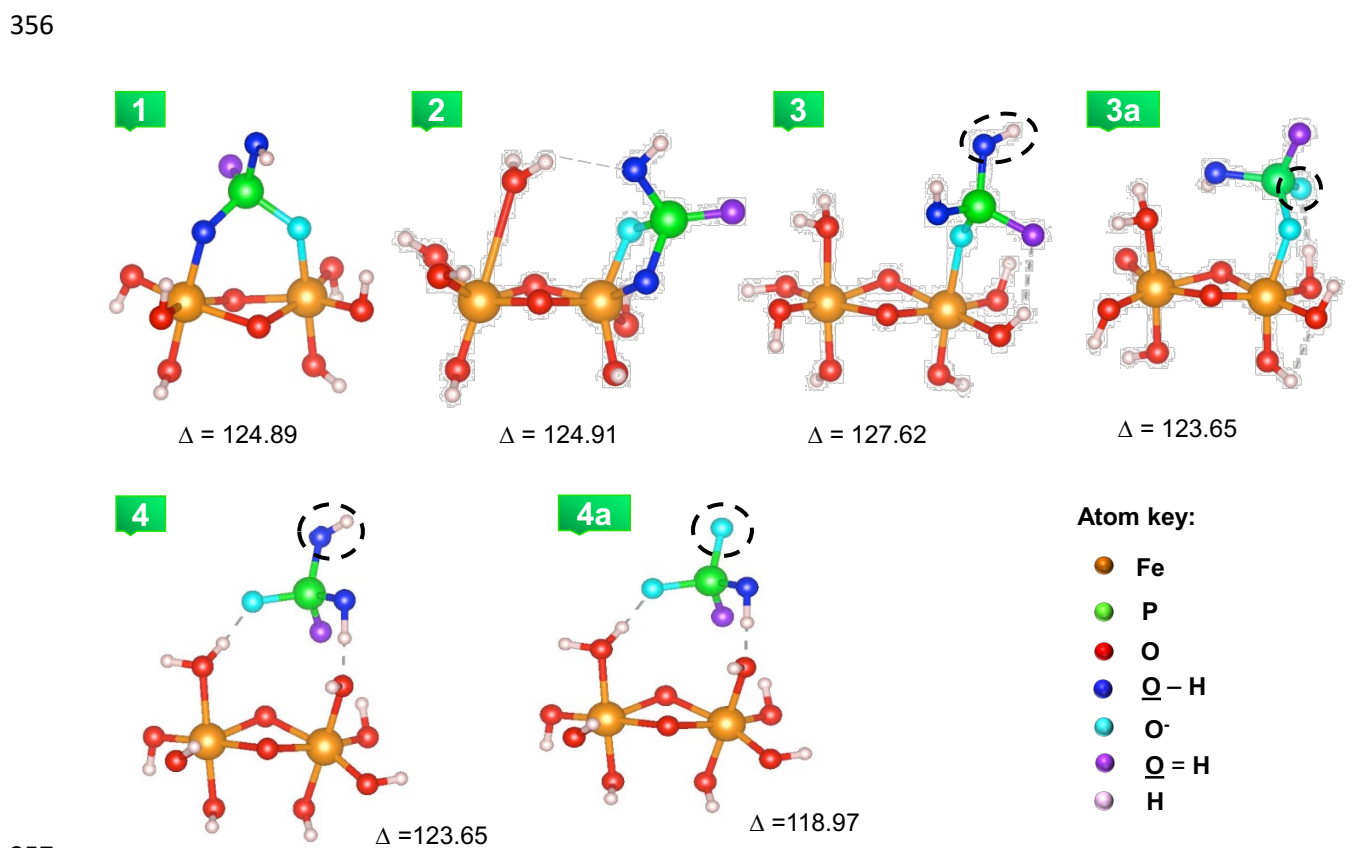
335 The adsorption kinetics of oxy-anions like P(V) with iron oxides/oxy-hydroxides were reported to
 336 follow pseudo-second-order kinetics that correlates with our experimental data as well (Figures
 337 6Aa and 6Ba).⁴³⁻⁴⁵ Initially, the phosphate adsorption with CM2LF and MAG occurs rapidly, but
 338 5 min onwards, it becomes slower (Supporting Information, Figure S4Aa and S5Aa). In our earlier
 339 studies⁴⁶, Raman spectroscopy measurements suggested pseudo-second-order kinetics for the
 340 adsorption of As(III/V) on CM2LF and MAG (Supporting Information, Figure S8). However, in
 341 the case of AP_{mix1}, P(V) and As(III) ions were competitive up to initial 15 min for CM2LF
 342 (Supporting Information, Figure S4Bb), but at a later stage, As(III) reached an equilibrium state
 343 earlier than P(V), both following the pseudo-second-order kinetics with two slopes and variable
 344 adsorption rates (Figure 6Ab). In the case of AP_{mix2}, As(V) clearly showed a faster rate than P(V)
 345 on CM2LF surface (Supporting Information, Figure S4Bc) showing similar kinetics behavior as
 346 former (Figure 6Ac). These results confirm the interference (or competition) between P(V) and
 347 As(III/V) species during adsorption on CM2LF.

348 **Table 1.** Adsorption data in terms of initial rates, rate constants and uptake of As at equilibrium.

Adsorbate 100 mL	Adsorbent (mg)	Species pH 7	q _e (mg/g) ± 1%	k (min(mg/g)) ⁻¹ ± 2%	Initial rate h = kq _e ² ± 5%	R ²
20 ppm P(V)	CM2LF: 100	H _x PO ₄ ^{y-}	18.26	0.02	6.67	0.99
	MAG: 100	H _x PO ₄ ^{y-}	15.83	0.02	5.01	0.99
5 ppm P(V)+ 5 ppmAs(III)	CM2LF: 100	H _x PO ₄ ^{y-}	3.39 (avg)	0.13 (avg)	1.49 (avg)	0.99
		H ₃ AsO ₃	2.67 (avg)	0.29 (avg)	2.07 (avg)	0.99
	MAG: 100	H _x PO ₄ ^{y-}	3.30	0.51	5.55	0.96
		H ₃ AsO ₃	2.28	0.28	1.45	0.99
5 ppm P(V)+	CM2LF: 100	H _x PO ₄ ^{y-}	3.06 (avg)	0.04 (avg)	0.37 (avg)	0.74
		H _x AsO ₄ ^{y-}	4.16 (avg)	0.05 (avg)	0.87 (avg)	0.99

5 ppm As(V)	MAG:	$H_xPO_4^{y-}$	2.30	1.64	8.67	0.99
	100	$H_xAsO_4^{y-}$	2.40	1.89	10.89	0.99

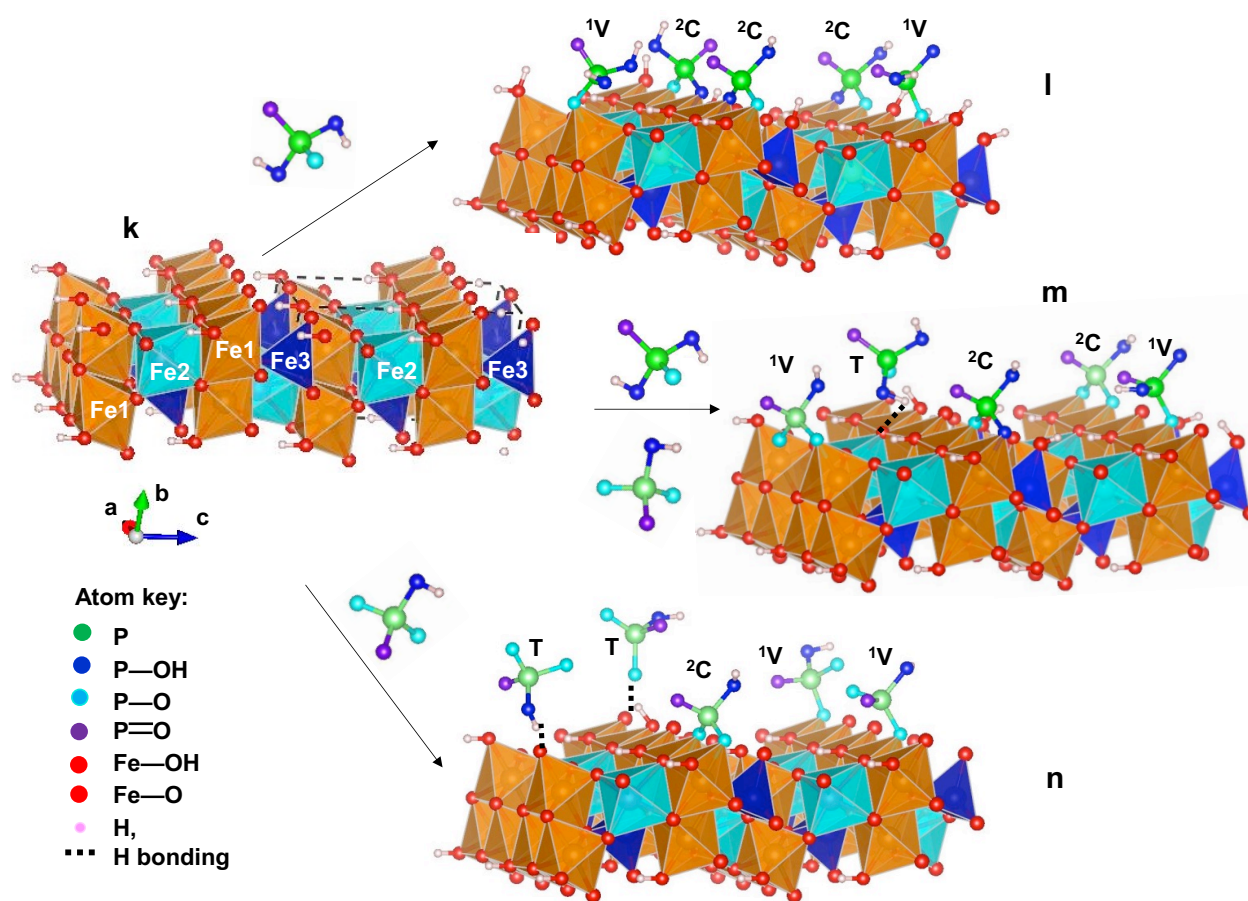
349
 350 In the case of magnetite, while P(V) adsorption was faster than As(III) initially (Supporting
 351 Information, Figure S5Bb), and after 10 min, desorption of P(V) was observed for AP_{mix1}.
 352 However, in the case of AP_{mix2}, both P(V) and As(V) showed comparable rates of adsorption
 353 throughout with higher As(V) uptake (Supporting Information, Figure S5Bc). Thus, As(III/V)
 354 show different adsorption kinetics for CM2LF and magnetite. Kinetics data are given in Table 1.
 355 These results are presented as a schematic diagram (Supporting Information, Figure S7).



357
 358 **Figure 7.** Various phosphate complexes with a small ferrihydrite cluster: (1) bidentate binuclear
 359 complex (²C), (2) bidentate mononuclear complex (²E), (3) monodentate mononuclear complex
 360 (¹V), (3a) deprotonated monodentate mononuclear complex (¹V-H), (4) outer-sphere complex (T),
 361 and (4a) Deprotonated outer-sphere complex (T-H). Here, theoretical binding energies ($\Delta = T_{BE2}$)
 362 of P 2p in phosphate complexes are reported in eV.

363 In order to understand the mechanism of adsorption of various phosphate species on CM2LF,
 364 theoretical studies were performed as discussed in Supporting Information. In Figure 7, to find the
 365 theoretical binding energy (T_{BE}) of P 2p in various complexes, equation $T_{BE2} = -E + R = \Delta$ was
 366 used⁴⁷ where E is the orbital energy, R is the relaxation energy and Δ is computed by Δ SCF
 367 method. Based on Δ , the binding energy of P 2p for the complexes given above follows the order,
 368 ${}^1V > {}^2E > {}^2C > {}^1V\text{-H} > T > T\text{-H}$ (Figure 7; Supporting Information, Table S2). Theoretical
 369 calculations of binding energy have been extended to As(III/V) complexes. Based on K, the
 370 binding energy of As 3d for the As(III) complexes follow the order, ${}^2C > {}^1V > {}^2E > T$ (Supporting
 371 Information, Figure S6). In the case of As(V) complexes, it follows the order, ${}^2E > {}^2C > {}^1V > T$
 372 (Supporting Information, Figure S6). The binding energies of As 3d for As(V) complexes are
 373 higher than As(III) complexes.

374



375

376 **Figure 8.** Schematic of a (010) plane of ferrihydrite (k) before adsorption, (l), (m), and (n) after
 377 phosphate adsorption at pH 5, 7, and 9, respectively.

378 To show phosphate adsorption on 2-line ferrihydrite schematically at various pH 5, 7 and 9
379 respectively, we used the unit cell parameters of 2-line ferrihydrite as reported in Michel et al.⁴⁸⁻
380 ⁴⁹. A rectangular slab was made with four unit cells and surfaces parallel to the (010) plane of
381 FeOOH (Figure 8). In general, the ferrihydrite structure has three symmetry-distinct Fe atoms.
382 Here, we represented them as octahedra Fe1 center (orange), octahedra Fe2 center (sky blue), and
383 tetrahedral Fe3 center (blue) as reported by Pinney et al.⁴⁹ The CM2LF -O-/-OH groups were
384 shown in red, while phosphorous attached -O⁻, -OH, and =O groups are marked in sky blue, blue,
385 and indigo, respectively. XPS and FTIR results suggest that phosphate species bind the surface Fe
386 atoms through a ligand exchange mechanism, at pH 5, 7. The results are supported by the
387 literature.^{28, 50-51} In the ligand exchange mechanism, -P-(O⁻/OH⁻) groups replace the Fe-(O⁻/OH⁻
388) groups. Moreover, the formation of possible stable complexes of phosphate with 2-line
389 ferrihydrite is shown in Figure 8. Herein, P(V) forms ²C (major), and ¹V (minor) complexes at pH
390 5 and 7 due to the presence of more labile groups Fe-(OH/OH₂⁺); on the other hand, at pH 9, P(V)
391 forms T (major), ²C(minor), and (¹V) (minor) complexes as result of increase of less labile groups
392 Fe-O⁻.

393

394 **Sustainability aspects of CM2LF and magnetite materials:**

395

396 To study the sustainability of CM2LF and magnetite systems, the following factors can be
397 considered: 1. Green synthesis, 2. Material efficiency, 3. Material stability and 4. Cost of
398 production. Upon carefully observing these factors for both the materials, CM2LF was found to
399 be a *greener* option than magnetite, owing to its ease and waterborne synthesis, higher arsenic
400 uptake capacity, mechanical robustness and cost-effective production process. Each aspect is
401 discussed in quantitative detail in SI.

402

403 **CONCLUSIONS**

404 Of the phosphate ions, H₂PO₄¹⁻ is dominant at pH 5 and HPO₄²⁻ is dominant at pH 9. Both species
405 exist in water at pH 7 as confirmed by ATR-FTIR studies. The P 2p binding energy of adsorbed
406 phosphate decreased gradually on CM2LF and MAG surfaces, upon increasing pH from 5 to 9.
407 The changes in P 2p energy levels suggest that surface complexes are varying with changes in pH.
408 The XPS and IR studies suggested that phosphate complexation with iron oxides/oxy-hydroxides

409 were driven by the ligand exchange mechanism, leading to the formation of Fe–O–P bonds at pH
410 5-7. The adsorbed materials showed P 2p binding energy in the order $AP_{mix2} > AP_{mix1} \geq$ phosphate
411 only samples. Time-dependent ion chromatography measurements allowed us to understand the
412 adsorption kinetics of As(III)/As(V) on CM2LF and MAG in presence P(V) at neutral pH. The
413 As(III)/As(V) adsorption kinetics was affected by phosphate . Phosphate desorbs from magnetite
414 in presence of As(III). At higher concentrations (i.e., 20 mM P(V) and 20 mM As(III/V)), XPS
415 data suggest that phosphate uptake by iron oxides/oxy-hydroxides gets affected by As(III) and
416 As(V). These studies confirm that As(III/V) is more competitive than P(V) towards iron
417 oxides/oxy-hydroxides. However, P(V) levels in natural water is 100-1000 times higher than that
418 of As(III/V), and therefore, P(V) is an obvious interfering ion during arsenic adsorption. DFT
419 calculations suggest that P 2p and As 3d binding energies vary with the type of complexation (2C ,
420 2E , 1V , and T). The degree protonation of P(V) in phosphate surface complexes affects the P 2p
421 binding energy. The binding energies of As 3d for As(V) complexes are higher than that of As(III)
422 complexes.

423

424 **ASSOCIATED CONTENT**

425 **Supporting Information**

426 Materials and instrumentation; 3D reconstructed tomographic images of 2-line ferrihydrite
427 composite (CM2LF) before and after arsenic adsorption; IR spectra of CM2LF treated in distilled
428 water at various pH; IR spectra of CM2LF after arsenic adsorption in presence of P(V); time-
429 dependent chromatograms of the interaction of CM2LF/magnetite with P(V)/ AP_{mix1} / AP_{mix2} ;
430 equations for pseudo-second-order model; theoretical binding energy of As 3d in various As(III/V)
431 complexes with a small ferrihydrite cluster; schematic illustration of P(V) interference on the
432 As(III/V) adsorption based on time dependent ion chromatography and XPS studies; pseudo-
433 second-order adsorption kinetic plots for the adsorption of As(III) and As(V) on ferrihydrite; XPS
434 data of materials before and after treatment with P(V), AP_{mix1} , and AP_{mix2} ; Sustainability aspects
435 of CM2LF and magnetite materials.

436

437

438

439 **AUTHOR INFORMATION**

440 Corresponding Author

441 *E-mail: pradeep@iitm.ac.in. Phone: +91-44 2257 4208. Fax:

442 +91-44 2257 0545/0509.

443 ORCID

444 Avula Anil Kumar: 0000-0001-6878-8736

445 Thalappil Pradeep: 0000-0003-3174-534X

446

447

448 **ACKNOWLEDGMENTS**

449

450 The authors thank IIT Madras and the Department of Science and Technology, Government of
451 India, for constantly supporting our research program on nanomaterials.

452

453 **REFERENCES**

- 454 1. Han, C.; Geng, J.; Ren, H.; Gao, S.; Xie, X.; Wang, X., Phosphite in Sedimentary Interstitial Water
455 of Lake Taihu, a Large Eutrophic Shallow Lake in China. *Environmental Science & Technology* **2013**, *47*,
456 5679-5685.
- 457 2. Park, S. W.; Kim, C. W.; Lee, J. H.; Shim, G.; Kim, K. S., Comparison of Arsenic Acid with
458 Phosphoric Acid in the Interaction with a Water Molecule and an Alkali/Alkaline-Earth Metal Cation. *The*
459 *Journal of Physical Chemistry A* **2011**, *115*, 11355-11361.
- 460 3. Wolfe-Simon, F.; Davies, P. C. W.; Anbar, A. D., Did Nature Also Choose Arsenic? *International*
461 *Journal of Astrobiology* **2009**, *8*, 69-74.
- 462 4. Nguyen, V. L.; Chen, W.-H.; Young, T.; Darby, J., Effect of Interferences on the Breakthrough of
463 Arsenic: Rapid Small Scale Column Tests. *Water Research* **2011**, *45*, 4069-4080.
- 464 5. Neupane, G.; Donahoe, R. J.; Arai, Y., Kinetics of Competitive Adsorption/Desorption of Arsenate
465 and Phosphate at the Ferrihydrite–Water Interface. *Chemical Geology* **2014**, *368*, 31-38.
- 466 6. Cagnasso, M.; Boero, V.; Franchini, M. A.; Chorover, J., Atr-Ftir Studies of Phospholipid Vesicle
467 Interactions with A-Feooh and A-Fe2o3 Surfaces. *Colloids and Surfaces B: Biointerfaces* **2010**, *76*, 456-
468 467.
- 469 7. Waychunas, G. A.; Rea, B. A.; Fuller, C. C.; Davis, J. A., Surface Chemistry of Ferrihydrite: Part
470 1. Exafs Studies of the Geometry of Coprecipitated and Adsorbed Arsenate. *Geochimica et Cosmochimica*
471 *Acta* **1993**, *57*, 2251-2269.
- 472 8. Hiemstra, T.; Van Riemsdijk, W. H., Surface Structural Ion Adsorption Modeling of Competitive
473 Binding of Oxyanions by Metal (Hydr)Oxides. *Journal of Colloid and Interface Science* **1999**, *210*, 182-
474 193.
- 475 9. Goldberg, S.; Johnston, C. T., Mechanisms of Arsenic Adsorption on Amorphous Oxides Evaluated
476 Using Macroscopic Measurements, Vibrational Spectroscopy, and Surface Complexation Modeling.
477 *Journal of Colloid and Interface Science* **2001**, *234*, 204-216.

- 478 10. Fukushi, K.; Sverjensky, D. A., A Predictive Model (Etlm) for Arsenate Adsorption and Surface
479 Speciation on Oxides Consistent with Spectroscopic and Theoretical Molecular Evidence. *Geochimica et*
480 *Cosmochimica Acta* **2007**, *71*, 3717-3745.
- 481 11. Neil, C. W.; Lee, B.; Jun, Y.-S., Different Arsenate and Phosphate Incorporation Effects on the
482 Nucleation and Growth of Iron(III) (Hydr)Oxides on Quartz. *Environmental Science & Technology* **2014**,
483 *48*, 11883-11891.
- 484 12. Tuutijärvi, T.; Repo, E.; Vahala, R.; Sillanpää, M.; Chen, G., Effect of Competing Anions on
485 Arsenate Adsorption onto Maghemite Nanoparticles. *Chinese Journal of Chemical Engineering* **2012**, *20*,
486 505-514.
- 487 13. Su, C.; Puls, R. W., Arsenate and Arsenite Removal by Zerovalent Iron: Effects of Phosphate,
488 Silicate, Carbonate, Borate, Sulfate, Chromate, Molybdate, and Nitrate, Relative to Chloride.
489 *Environmental Science & Technology* **2001**, *35*, 4562-4568.
- 490 14. Roberts, L. C.; Hug, S. J.; Ruettimann, T.; Billah, M. M.; Khan, A. W.; Rahman, M. T., Arsenic
491 Removal with Iron(II) and Iron(III) in Waters with High Silicate and Phosphate Concentrations.
492 *Environmental Science & Technology* **2004**, *38*, 307-315.
- 493 15. Mallet, M.; Barthélémy, K.; Ruby, C.; Renard, A.; Naille, S., Investigation of Phosphate
494 Adsorption onto Ferrihydrite by X-Ray Photoelectron Spectroscopy. *Journal of Colloid and Interface*
495 *Science* **2013**, *407*, 95-101.
- 496 16. Tofan-Lazar, J.; Al-Abadleh, H. A., Kinetic Atr-Ftir Studies on Phosphate Adsorption on Iron
497 (Oxyhydr)Oxides in the Absence and Presence of Surface Arsenic: Molecular-Level Insights into the
498 Ligand Exchange Mechanism. *The Journal of Physical Chemistry A* **2012**, *116*, 10143-10149.
- 499 17. Kwon, K. D.; Kubicki, J. D., Molecular Orbital Theory Study on Surface Complex Structures of
500 Phosphates to Iron Hydroxides: Calculation of Vibrational Frequencies and Adsorption Energies. *Langmuir*
501 **2004**, *20*, 9249-9254.
- 502 18. Kim, J.; Li, W.; Philips, B. L.; Grey, C. P., Phosphate Adsorption on the Iron Oxyhydroxides
503 Goethite (A-Feooh), Akaganeite (B-Feooh), and Lepidocrocite (Γ-Feooh): A ³¹P Nmr Study. *Energy &*
504 *Environmental Science* **2011**, *4*, 4298-4305.
- 505 19. Almasri, D. A.; Saleh, N. B.; Atieh, M. A.; McKay, G.; Ahzi, S., Adsorption of Phosphate on Iron
506 Oxide Doped Halloysite Nanotubes. *Scientific Reports* **2019**, *9*, 3232.
- 507 20. Karunanayake, A. G.; Navarathna, C. M.; Gunatilake, S. R.; Crowley, M.; Anderson, R.; Mohan,
508 D.; Perez, F.; Pittman, C. U.; Mlsna, T., Fe₃O₄ Nanoparticles Dispersed on Douglas Fir Biochar for
509 Phosphate Sorption. *ACS Applied Nano Materials* **2019**, *2*, 3467-3479.
- 510 21. Wang, T.; Xu, X.; Ren, Z.; Gao, B.; Wang, H., Adsorption of Phosphate on Surface of Magnetic
511 Reed: Characteristics, Kinetic, Isotherm, Desorption, Competitive and Mechanistic Studies. *RSC Advances*
512 **2016**, *6*, 5089-5099.
- 513 22. Arai, Y.; Sparks, D. L., Atr-Ftir Spectroscopic Investigation on Phosphate Adsorption Mechanisms
514 at the Ferrihydrite-Water Interface. *Journal of Colloid and Interface Science* **2001**, *241*, 317-326.
- 515 23. Kubicki, J. D.; Paul, K. W.; Kaban, L.; Zhu, Q.; Mroziak, M. K.; Aryanpour, M.; Pierre-Louis, A.-
516 M.; Strongin, D. R., Atr-Ftir and Density Functional Theory Study of the Structures, Energetics, and
517 Vibrational Spectra of Phosphate Adsorbed onto Goethite. *Langmuir* **2012**, *28*, 14573-14587.
- 518 24. Han, J.; Ro, H.-M., Characterizing Preferential Adsorption of Phosphate on Binary Sorbents of
519 Goethite and Maghemite Using in Situ Atr-Ftir and 2d Correlation Spectroscopy. *Scientific Reports* **2019**,
520 *9*, 6130.
- 521 25. Elzinga, E. J.; Sparks, D. L., Phosphate Adsorption onto Hematite: An in Situ Atr-Ftir Investigation
522 of the Effects of Ph and Loading Level on the Mode of Phosphate Surface Complexation. *Journal of Colloid*
523 *and Interface Science* **2007**, *308*, 53-70.
- 524 26. Wang, Z.; Giammar, D. E., Mass Action Expressions for Bidentate Adsorption in Surface
525 Complexation Modeling: Theory and Practice. *Environmental Science & Technology* **2013**, *47*, 3982-3996.
- 526 27. Ta, H. T. T.; Tieu, A. K.; Zhu, H.; Yu, H.; Ta, T. D.; Wan, S.; Tran, N. V.; Le, H. M., Chemical
527 Origin of Sodium Phosphate Interactions on Iron and Iron Oxide Surfaces by First Principle Calculations.
528 *The Journal of Physical Chemistry C* **2018**, *122*, 635-647.

529 28. Daou, T. J.; Begin-Colin, S.; Grenèche, J. M.; Thomas, F.; Derory, A.; Bernhardt, P.; Legaré, P.;
530 Pourroy, G., Phosphate Adsorption Properties of Magnetite-Based Nanoparticles. *Chemistry of Materials*
531 **2007**, *19*, 4494-4505.

532 29. Carabante, I.; Grahn, M.; Holmgren, A.; Hedlund, J., In Situ Atr–Ftir Studies on the Competitive
533 Adsorption of Arsenate and Phosphate on Ferrihydrite. *Journal of Colloid and Interface Science* **2010**, *351*,
534 523-531.

535 30. Zeng, H.; Fisher, B.; Giammar, D. E., Individual and Competitive Adsorption of Arsenate and
536 Phosphate to a High-Surface-Area Iron Oxide-Based Sorbent. *Environmental Science & Technology* **2008**,
537 *42*, 147-152.

538 31. Kumar, A. A., et al., Confined Metastable 2-Line Ferrihydrite for Affordable Point-of-Use Arsenic-
539 Free Drinking Water. *Advanced Materials* **2017**, *29*, 1604260.

540 32. Worden, R. H., Analytical Methods | Geochemical Analysis (Including X-Ray). In *Encyclopedia*
541 *of Geology*, Selley, R. C.; Cocks, L. R. M.; Plimer, I. R., Eds. Elsevier: Oxford, 2005; pp 54-76.

542 33. Hou, L.; Liang, Q.; Wang, F., Mechanisms That Control the Adsorption–Desorption Behavior of
543 Phosphate on Magnetite Nanoparticles: The Role of Particle Size and Surface Chemistry Characteristics.
544 *RSC Advances* **2020**, *10*, 2378-2388.

545 34. Tejedor-Tejedor, M. I.; Anderson, M. A., The Protonation of Phosphate on the Surface of Goethite
546 as Studied by Cir-Ftir and Electrophoretic Mobility. *Langmuir* **1990**, *6*, 602-611.

547 35. Sassi, M.; Rosso, K. M., Roles of Hydration and Magnetism on the Structure of Ferrihydrite from
548 First Principles. *ACS Earth and Space Chemistry* **2019**, *3*, 70-78.

549 36. Erbs, J. J.; Gilbert, B.; Penn, R. L., Influence of Size on Reductive Dissolution of Six-Line
550 Ferrihydrite. *The Journal of Physical Chemistry C* **2008**, *112*, 12127-12133.

551 37. Dzombak, D. A.; François M. M. Morel., Surface Complexation Modeling: Hydrous Ferric Oxide.
552 *John Wiley & Sons*, New York, **1990**.

553 38. Persson, P.; Nilsson, N.; Sjöberg, S., Structure and Bonding of Orthophosphate Ions at the Iron
554 Oxide–Aqueous Interface. *Journal of Colloid and Interface Science* **1996**, *177*, 263-275.

555 39. Grosvenor, A. P.; Kobe, B. A.; Biesinger, M. C.; McIntyre, N. S., Investigation of Multiplet
556 Splitting of Fe 2p Xps Spectra and Bonding in Iron Compounds. *Surface and Interface Analysis* **2004**, *36*,
557 1564-1574.

558 40. Wang, X.; Hu, Y.; Tang, Y.; Yang, P.; Feng, X.; Xu, W.; Zhu, M., Phosphate and Phytate
559 Adsorption and Precipitation on Ferrihydrite Surfaces. *Environmental Science: Nano* **2017**, *4*, 2193-2204.

560 41. Abdala, D. B.; Northrup, P. A.; Arai, Y.; Sparks, D. L., Surface Loading Effects on Orthophosphate
561 Surface Complexation at the Goethite/Water Interface as Examined by Extended X-Ray Absorption Fine
562 Structure (Exafs) Spectroscopy. *Journal of Colloid and Interface Science* **2015**, *437*, 297-303.

563 42. Beji, Z.; Sun, M.; Smiri, L. S.; Herbst, F.; Mangeney, C.; Ammar, S., Polyol Synthesis of Non-
564 Stoichiometric Mn–Zn Ferrite Nanocrystals: Structural /Microstructural Characterization and Catalytic
565 Application. *RSC Advances* **2015**, *5*, 65010-65022.

566 43. Chandra, V.; Park, J.; Chun, Y.; Lee, J. W.; Hwang, I.-C.; Kim, K. S., Water-Dispersible Magnetite-
567 Reduced Graphene Oxide Composites for Arsenic Removal. *ACS Nano* **2010**, *4*, 3979-3986.

568 44. Kumar, S.; Nair, R. R.; Pillai, P. B.; Gupta, S. N.; Iyengar, M. A. R.; Sood, A. K., Graphene Oxide–
569 Mnfe2o4 Magnetic Nanohybrids for Efficient Removal of Lead and Arsenic from Water. *ACS Applied*
570 *Materials & Interfaces* **2014**, *6*, 17426-17436.

571 45. Yang, J.-C.; Yin, X.-B., Cofe2o4@Mil-100(Fe) Hybrid Magnetic Nanoparticles Exhibit Fast and
572 Selective Adsorption of Arsenic with High Adsorption Capacity. *Scientific Reports* **2017**, *7*, 40955.

573 46. Sudhakar, C.; Anil Kumar, A.; Bhuin, R. G.; Sen Gupta, S.; Natarajan, G.; Pradeep, T., Species-
574 Specific Uptake of Arsenic on Confined Metastable 2-Line Ferrihydrite: A Combined Raman-X-Ray
575 Photoelectron Spectroscopy Investigation of the Adsorption Mechanism. *ACS Sustainable Chemistry &*
576 *Engineering* **2018**, *6*, 9990-10000.

577 47. Tardio, S.; Cumpson, P. J., Practical Estimation of Xps Binding Energies Using Widely Available
578 Quantum Chemistry Software. *Surface and Interface Analysis* **2018**, *50*, 5-12.

579 48. Michel, F. M.; Ehm, L.; Antao, S. M.; Lee, P. L.; Chupas, P. J.; Liu, G.; Strongin, D. R.; Schoonen,
580 M. A. A.; Phillips, B. L.; Parise, J. B., The Structure of Ferrihydrite, a Nanocrystalline Material. *Science*
581 **2007**, *316*, 1726.

582 49. Pinney, N.; Kubicki, J. D.; Middlemiss, D. S.; Grey, C. P.; Morgan, D., Density Functional Theory
583 Study of Ferrihydrite and Related Fe-Oxyhydroxides. *Chemistry of Materials* **2009**, *21*, 5727-5742.

584 50. Antelo, J.; Avena, M.; Fiol, S.; López, R.; Arce, F., Effects of Ph and Ionic Strength on the
585 Adsorption of Phosphate and Arsenate at the Goethite–Water Interface. *Journal of Colloid and Interface*
586 *Science* **2005**, *285*, 476-486.

587 51. Antelo, J.; Fiol, S.; Pérez, C.; Mariño, S.; Arce, F.; Gondar, D.; López, R., Analysis of Phosphate
588 Adsorption onto Ferrihydrite Using the Cd-Music Model. *Journal of Colloid and Interface Science* **2010**,
589 *347*, 112-119.

590

591

592

593

594

595

596

597

598

599

600

601

602

603

604

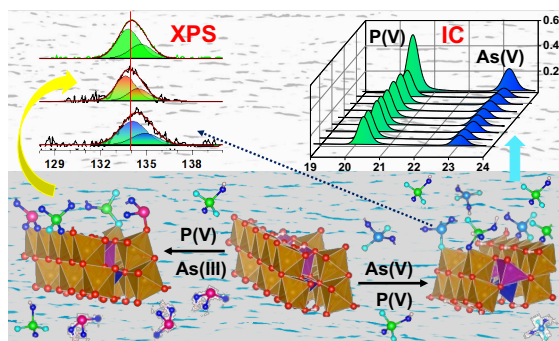
605

606

TOC Graphic

607 **Title:** Interference of Phosphate on the Adsorption of Arsenate and Arsenite Over Confined
608 Metastable 2-Line Ferrihyrite and Magnetite

609 **Authors:** Chennu Sudhakar, Sritama Mukherjee, Avula Anil Kumar, Ganesan Paramasivam,
610 Karthigai Meena P, Nonappa, and Thalappil Pradeep



611

612

613